• Basic Research •

Inhibition of TOP2A by columbianadin impedes malignant progression in retinoblastoma

Lu-Jun Li[1], *He Sun*[2], *Zhong-Hua Tang*[3], *Ming-Yuan Xu*[1]

[1]Department of Pharmacy, the First Affiliated Hospital of Heilongjiang University of Chinese Medicine, Harbin 150040, Heilongjiang Province, China
[2]Department of Ophthalmology, the First Affiliated Hospital of Heilongjiang University of Chinese Medicine, Harbin 150040, Heilongjiang Province, China
[3]College of Chemistry, Chemical Engineering and Resource Utilization, Northeast Forestry University, Harbin 150040, Heilongjiang Province, China
Correspondence to: Ming-Yuan Xu. Department of Pharmacy, the First Affiliated Hospital of Heilongjiang University of Chinese Medicine, Harbin 150040, Heilongjiang Province, China. xumingyuan@hljucm.edu.cn
Received: 2025-10-23 Accepted: 2026-08-03

Abstract

● **AIM:** To investigate the molecular mechanism by which columbianadin (CBN) exerts its antitumor effects in retinoblastoma (RB).

● **METHODS:** Y79 and WERI-Rb-1 cells were used for *in vitro* assays. Cell viability under different concentrations of CBN was assessed. The effects of CBN on RB cell behaviors were examined. *In vivo,* the antitumor efficacy of CBN was evaluated using a xenograft tumor model in BALB/c nude mice. Bioinformatic analysis was performed to predict potential molecular targets of CBN. The role of DNA topoisomerase II alpha (TOP2A) in activating the phosphoinositide 3-kinase/protein kinase B (PI3K/AKT) signaling pathway was further explored. RB cells were infected with a lentivirus to overexpress TOP2A or treated with a PI3K/AKT inhibitor to analyze cellular behavior. A xenograft model was established using Y79 cells overexpressing TOP2A to validate the *in vitro* findings under CBN treatment.

● **RESULTS:** CBN inhibited proliferation, migration, and invasion, and promoted apoptosis of Y79 and WERI-Rb-1 cells. *In vivo,* CBN markedly reduced tumor growth in nude mice. TOP2A was highly expressed in RB cells, and its expression was downregulated by CBN treatment. Mechanistically, TOP2A promoted the malignant behavior of RB cells and tumor growth by activating the PI3K/AKT pathway.

● **CONCLUSION:** CBN inhibits RB progression by downregulating TOP2A protein expression, thereby blocking activation of the PI3K/AKT signaling pathway. These findings suggest that CBN could be a viable therapeutic candidate for treating RB.

● **KEYWORDS:** columbianadin; topoisomerase II alpha; phosphoinositide 3-kinase/protein kinase B signaling pathway; retinoblastoma; tumor progression

DOI:10.18240/ijo.2026.11.05

Citation: Li LJ, Sun H, Tang ZH, Xu MY. Inhibition of TOP2A by columbianadin impedes malignant progression in retinoblastoma. *Int J Ophthalmol* 2026;19(11):2135-2147

INTRODUCTION

Retinoblastoma (RB) is the most common malignant intraocular tumor in children, with an incidence of 1 in 18 000 live births[1]. RB is initiated primarily by inactivation of both alleles of the *RB1* tumor suppressor gene, but its pathogenesis involves complex molecular events beyond *RB1* loss[2]. Current RB management strategies include systemic or intra-arterial chemotherapy[3] and focal therapies (cryotherapy, laser photocoagulation, thermotherapy)[4] for advanced cases. While these approaches can achieve tumor control, they have notable limitations: systemic toxicity, risk of secondary malignancies, and incomplete eradication of tumor cells that can lead to relapse[5]. There are pressing, unresolved concerns regarding the diagnosis, treatment, and enhancement of quality of life for patients and their families[6].

Columbianadin (CBN), a dihydroangelic acid ester and naturally occurring coumarin compound, is primarily derived from plants in the *Apiaceae* family and exhibits a broad spectrum of bioactivities, including neuroprotective, antitumor, anti-inflammatory, and analgesic effects[7]. CBN has been shown to suppress the progression of several malignancies, such as glioblastoma, by modulating cell proliferation, invasion, and apoptosis[8]. However, whether CBN exerts therapeutic effects in RB and the mechanisms involved remain unexplored.

Topoisomerase II-alpha (TOP2A), an essential nuclear enzyme involved in DNA replication, transcription, and chromosome

segregation, is frequently upregulated in various cancers and is linked to high proliferative activity, tumor aggressiveness, and poor prognosis[9]. For example, TOP2A is highly expressed in ophthalmic tumors and strongly associated with ophthalmic tumorigenesis[10]. Even though β-carboline derivatives have been recently shown to be promising dual-target inhibitors of DNA and TOP2A for the treatment of triple-negative breast cancer[11], the specific role of TOP2A in RB has not been elucidated. Notably, TOP2A drives prostate cancer cell malignant phenotypes by activating the phosphoinositide 3-kinase/protein kinase B (PI3K/AKT) signaling pathway[12]. Dysregulation of the PI3K/AKT pathway has been implicated in RB progression, and inhibition of this pathway can suppress RB cell growth[13]. Moreover, CBN ameliorated myocardial injury by inhibiting the PI3K/AKT mechanistic target of rapamycin (mTOR) signaling pathway in mice[14]. Therefore, targeting TOP2A and the downstream PI3K/AKT axis may represent a novel therapeutic approach for RB.

Based on these observations, we hypothesize that CBN suppresses the malignant behaviors of RB cells by downregulating TOP2A expression and inactivating the PI3K/AKT signaling pathway. The results of this study offer a novel perspective on the anticancer potential of CBN and underscore its significance as a potential candidate compound for RB therapy.

MATERIALS AND METHODS

Ethical Approval All animal procedures were approved by the Animal Care and Use Committee of Heilongjiang University of Chinese Medicine (approval number: 2024122902).

Cell Models The RB cell lines Y79 (catalog No.SNL-532, SUNCELL Biological Technology, Wuhan, China) and WERI-Rb-1 (catalog No.SNL-470, SUNCELL Biological Technology) were cultured in RPMI-1640 medium (catalog No.11875119, Thermo Fisher Scientific, Waltham, MA, USA) supplemented with 10% fetal bovine serum and 1% penicillin–streptomycin. Adult retinal pigment epithelial cell line-19 (ARPE-19, catalog No.SNL-227, SUNCELL Biological Technology) was cultured in Dulbecco's Modified Eagle Medium/*F*-12 (catalog No.11320033, Thermo Fisher Scientific, USA) containing the same supplements. All cells were maintained at 37°C in a humidified atmosphere containing 5% CO_2, and the culture medium was replaced every three days.

RB cells were seeded at 37°C in medium containing 5 μg/mL polybrene and transduced with lentivirus overexpressing TOP2A or control empty vector lentivirus (Cyagen Biosciences, Shanghai, China) at a multiplicity of infection of 5. After 48h, RB cells were subjected to continuous screening with 2 μg/mL puromycin for 7d. After screening, TOP2A protein expression was detected *via* Western blot (WB) analysis to verify the efficiency of TOP2A overexpression. The stably infected cells were then used for the following experiments.

RB cells were treated with various concentrations (0, 10, 20, 30, 40, and 50 μmol/L) of CBN (purity: 99.97%, catalog No.S9017, Selleck Chemicals, Houston, TX, USA) for 24h. CBN was dissolved in dimethyl sulfoxide (DMSO) and diluted with cell culture medium to the desired working concentration. The final concentration of DMSO was consistent across all CBN treatment groups and their corresponding vehicle control groups, remaining below 0.1% (v/v). For the PI3K/AKT pathway inhibition assay, RB cells were treated with 50 nmol/L LY294002 (purity: 99.99%, catalog No.S1105, Selleck Chemicals, USA), a PI3K inhibitor, along with CBN, while control groups received an equal volume of DMSO at the same final concentration.

Cell Viability Assay RB and ARPE-19 cell viability following CBN treatment was assessed using the cell counting kit-8 (CCK-8; catalog No.MX3008-5ML, Maokang Biotechnology, Shanghai, China). The cells were seeded at 5000 cells/well in 96-well plates and incubated for 24h before treatment with 0–50 μmol/L CBN. Then, 10 μL of CCK-8 solution was added to each well and incubated for 2h. Absorbance was measured at 450 nm using a microplate reader.

EdU Assay Cell proliferation was evaluated using the VaClick 647-5-ethynyl-2'-deoxyuridine (EdU) cell proliferation test kit (catalog No.A413-01, Vazyme Biotech, Nanjing, China). Treated RB cells were seeded at 1×10^5 cells/well in 96-well plates and incubated with 10 μmol/L EdU solution for 2h. After being fixed with 4% paraformaldehyde (PFA) for 5min, the cells were incubated with 2 mg/mL glycine (100 μL) for 5min, permeabilized with 0.5% Triton X-100 (100 μL) for 10min, and stained with 100 μL Hoechst 33342 staining solution in the dark for 10min (all at room temperature). Images were observed and acquired using a fluorescence microscope.

Soft Agar Colony Formation Assay A 1% low-melting-point agarose solution was mixed with an equal volume of RB complete medium, and 1.5 mL of the mixture was added to the bottom of a 6-well plate. Treated RB cells (5000 cells/well) were suspended in complete medium and mixed at a ratio of 1:1 with 0.6% agarose solution. Plates were overlaid with 1.5 mL of the agar–medium mixture and incubated for 14d. Colonies containing>50 cells were counted under a microscope.

Transwell Assays RB cell migration and invasion were assessed using 24-well Transwell chambers with 8.0 μm pore polycarbonate membranes (catalog No.3422, Corning Inc., Corning, NY, USA). For invasion assays, membranes were pre-coated with Matrigel (catalog No.354234, Corning Inc. NY, USA). RB cell (5×10^4; 100 μL) suspension was seeded into the apical chambers, and the basolateral chambers contained RPMI-1640 with 10% fetal bovine serum. After 48h, invaded or migrated cells were fixed with 4% PFA for 20min, stained with crystal violet for 20min, and counted under a microscope.

Terminal Deoxynucleotidyl Transferase dUTP Nick-end Labeling Assay Apoptosis was analyzed using the YSFluor 488 transferase dUTP nick-end labeling (TUNEL) apoptosis detection kit (catalog No.40307ES20, YEASEN Biotechnology, Shanghai, China). RB cells were resuspended in phosphate-buffered saline (PBS) at 2×10^7 cells/mL, and 100 μL of the cell suspension was dropped onto a glass slide. The cells were fixed with a 4% PFA solution at 4℃ for 25min. The samples were incubated with Proteinase K solution and 1×equilibration buffer, and with 50 μL of TdT incubation buffer at 37℃ for 1h in the dark. Next, under dark conditions, slides were immersed in 4',6-diamidino-2-phenylindole and incubated at room temperature for 5min. The samples were observed under a fluorescence microscope.

Xenograft Tumor Model Four-week-old female BALB/c nude mice were purchased from Hunan SJA Laboratory Animal Co., Ltd. (Changsha, Hunan, China) and maintained under standard conditions. A 1:1 mixture of PBS and Matrigel containing 8×10^6 Y79 cell suspension was injected subcutaneously into the right flank of nude mice. CBN was prepared as a uniform suspension using 0.5% CMC-Na and diluted to the appropriate concentration. CBN treatment began when tumors reached 200 mm^3. The nude mice were treated by intraperitoneal injection with low, medium, or high doses of CBN (10, 20, or 40 mg/kg) or an equal volume of CMC-Na solution (vehicle), twice weekly for three weeks. Tumor volume was measured weekly using the formula: volume=(length×$width^2$)/2. After 3wk of treatment with CBN, nude mice were euthanized with sodium pentobarbital (150 mg/kg), and tumors were harvested.

***In vivo* Safety Assessment** To evaluate the short-term *in vivo* safety of CBN in normal nude mice, an additional 4-week-old female BALB/c nude mice were randomly divided into a Vehicle group and an H-CBN group, with 5 mice in each group. Mice in the H-CBN group were administered 40 mg/kg of CBN *via* intraperitoneal injection, while those in the Vehicle group received an equal volume of 0.5% CMC-Na vehicle solution, twice weekly for 3 consecutive weeks. The body weight changes of the nude mice were recorded weekly during the dosing period. After the administration was completed, the nude mice were euthanized by intraperitoneal injection of 150 mg/kg sodium pentobarbital, and heart, liver, spleen, lung, and kidney tissues were collected. The tissues were fixed in 4% PFA, embedded in paraffin, and sectioned, followed by hematoxylin-eosin (HE) staining. The histological structures of the major organs were then examined under a light microscope.

Immunohistochemistry Tumor paraffin-embedded sections (5 μm thickness) were deparaffinized, rehydrated, and subjected to antigen retrieval in sodium citrate buffer at 80℃ for 15min, followed by endogenous peroxidase blocking with 3% hydrogen peroxide for 15min. Sections were sealed with 5% goat serum for 45min and incubated overnight at 4℃ with primary antibodies and with the secondary antibody at room temperature for 45min. Visualization was performed using a 3,3'-diaminobenzidine substrate kit (catalog No.BL732A, Biosharp Life Sciences, Hefei, Anhui, China), followed by hematoxylin counterstaining. Dehydrated and mounted slides were observed under a microscope and analyzed with ImageJ software for relative integrated optical density (IOD).

Primary antibodies used in immunohistochemistry (IHC): anti-Ki67 (1:200, catalog No.A20018, ABclonal Technology, Wuhan, Hubei, China) and anti-TOP2A (1:100, catalog No.ab52934, Abcam, Cambridge, UK). Horseradish peroxidase-conjugated goat anti-rabbit IgG (H+L; 1:50, catalog No.AS014, ABclonal Technology) was used.

Western Blot Tumor tissues and RB cells were lysed in radioimmunoprecipitation assay buffer (catalog No.20101ES60, YEASEN Biotechnology) containing 1% protease inhibitors for 20min on ice. Protein concentrations were determined using the bicinchoninic acid protein assay kit (catalog No.BCA1, Sigma-Aldrich, St. Louis, MO, USA). Equal amounts of protein were separated by 8%–10% sodium dodecyl sulfate-polyacrylamide gel electrophoresis, transferred to polyvinylidene fluoride membranes, blocked with 5% bovine serum albumin for 2h at room temperature, and incubated overnight at 4℃ with primary antibodies. Membranes were incubated with horseradish peroxidase-conjugated goat anti-rabbit IgG (H+L; 1:2,000, catalog No.AS014, ABclonal Technology) for 1h at room temperature. Signals were detected using an enhanced chemiluminescence kit (catalog No.PK10001, Proteintech Group, Inc., Rosemont, IL, USA) and analyzed using ImageJ. Glyceraldehyde-3-phosphate dehydrogenase (GAPDH) served as the loading control.

Primary antibodies used in WB were: anti-Bax (1:20 000, catalog No.50599-2-Ig, Proteintech); anti-Bcl-2 (1:5000, catalog No.80313-1-RR, Proteintech); anti-TOP2A (1:10 000, catalog No.ab52934, Abcam); anti-PI3K (1:1000, catalog No.30092-1-AP, Proteintech); anti-phospho-PI3K (p-PI3K; 1:500, catalog No.PA5-104853, Thermo Fisher Scientific); anti-AKT (1:1000, catalog No.A17909, ABclonal Technology); anti-phospho-AKT (p-AKT; 1:500, catalog No.AP0637, ABclonal Technology); anti-GAPDH (1:1000, catalog No.ab313650, Abcam).

Reverse Transcription Quantitative Polymerase Chain Reaction Total RNA was isolated from Y79 and WERI-Rb-1 cells using the FastPure Cell/Tissue Total RNA Isolation Kit V2 (RC112, Vazyme), and the RNA concentration and purity were determined using a micro-spectrophotometer. An equal volume of total RNA was reverse-transcribed into cDNA using

Table 1 Primer sequence

Name	Forward	Reverse
TOP2A	5′-GTGGCAAGGATTCTGCTAGTCC-3′	5′-ACCATTCAGGCTCAACACGCTG-3′
GAPDH	5′-GTCTCCTCTGACTTCAACAGCG-3′	5′-ACCACCCTGTTGCTGTAGCCAA-3′

TOP2A: Topoisomerase II alpha; GAPDH: Glyceraldehyde-3-phosphate dehydrogenase.

HiScript III RT SuperMix for quantitative polymerase chain reaction (qPCR; R323, Vazyme). Real-time quantitative PCR was performed using ChamQ Universal SYBR qPCR Master Mix (Q711, Vazyme), with amplification and fluorescence signal detection carried out on a LightCycler 480 Instrument II (Roche Diagnostics, Co., Ltd., Rotkreuz, Switzerland). The results were normalized to GAPDH expression. The specific primers used are listed in Table 1. For the analysis of amplification results, relative fold changes were calculated using the $2^{-\Delta\Delta Ct}$ method.

Molecular Docking The three-dimensional structure file of the TOP2A protein (PDB ID: 1ZXM) was obtained from the Protein Data Bank database (https://www.rcsb.org/). The structural information for CBN was downloaded from the PubChem database (CID: 6436246), and its three-dimensional conformation was constructed based on its SMILES structural formula. Molecular docking analysis was performed using the DeepMice online platform (https://www.deepmice.com/) with the AutoDock Vina algorithm. Docking scores were evaluated using the minimum binding free energy (best_vina_score) output by AutoDock Vina. The docking result with the lowest binding energy and a reasonable conformation was selected. After the alignment was complete, the optimal protein-ligand complex conformation was imported into PyMOL for visualization. Combined with the interaction analysis results output by DeepMice, the key amino acid residues in the CBN-TOP2A binding pocket and their noncovalent interactions were annotated and organized.

Statistical Analysis Statistical analyses were performed using GraphPad Prism version 10.3.1 (GraphPad Software, San Diego, CA, USA). Data are presented as mean±standard error of the mean. The concentration-response curve for CBN was fitted using nonlinear regression analysis, and the IC_{50} value was calculated based on this. All measurement data were first assessed for normality using the Shapiro-Wilk test. For data that followed a normal distribution, the *F*-test was used to assess homogeneity of variances when comparing two groups, and the Brown-Forsythe test was used for comparisons involving multiple groups. For data that followed a normal distribution with homogeneous variances, an unpaired *t*-test was used for comparisons between two groups; an ordinary one-way analysis of variance (ANOVA) and an ordinary two-way ANOVA, followed by Tukey's multiple comparisons test, were used for comparisons among multiple groups. All experiments were performed in triplicate using independent biological replicates, and animal experiments included five mice per group. A P-value<0.05 was considered statistically significant.

RESULTS

CBN Inhibits the Malignant Phenotype and Promotes Apoptosis in RB Cells Y79 and WERI-Rb-1 cells were treated with CBN at 0, 10, 20, 30, 40, and 50 μmol/L for 24h, and cell viability was assessed by the CCK-8 assay. CBN reduced the viability of two RB cell lines in a concentration-dependent manner. Nonlinear fitting of the concentration-response curve for CBN on RB cell viability revealed that the IC_{50} values for CBN were 46.01 and 41.22 μmol/L for Y79 and WERI-Rb-1 cells, respectively (Figure 1A). Given that 50 μmol/L was close to the IC_{50} for Y79 cells and slightly higher than the IC_{50} for WERI-Rb-1 cells, we selected 50 μmol/L of CBN for subsequent experiments to ensure a relatively consistent and distinct inhibitory effect in both RB cell lines.

CCK-8 results further showed that ARPE-19 cell viability did not decrease significantly after 24h of treatment with 0–50 μmol/L CBN, suggesting that 50 μmol/L CBN did not exhibit significant cytotoxicity toward ARPE-19 cells (Figure 1B).

The EdU assay demonstrated that CBN reduced the percentage of EdU-positive RB cells, indicating that CBN inhibited RB cell proliferation (Figure 1C). Additionally, the soft agar colony formation assay confirmed that after treatment with CBN, the colony-forming ability of RB cells was weakened (Figure 1D). Transwell assay results showed that CBN treatment inhibited the migration and invasion of RB cells (Figure 1E, 1F). The TUNEL assay indicated that CBN promoted apoptosis in RB cells (Figure 1G).

CBN Exerts Antitumor Effects *in vivo* and Demonstrates Preliminary Systemic Safety A subcutaneous xenograft model was established by injecting Y79 cells into nude mice, followed by treatment with graded doses of CBN (10, 20, or 40 mg/kg) or Vehicle control. CBN slowed tumor growth, as evidenced by reduced tumor volume and weight (Figure 2A, 2B). IHC analysis revealed a marked decrease in the proliferation marker Ki67 in tumor tissues after CBN treatment (Figure 2C). WB analysis showed that CBN downregulated the anti-apoptotic protein Bcl-2 and upregulated the pro-apoptotic protein Bax in tumor tissues (Figure 2D). Among the tested

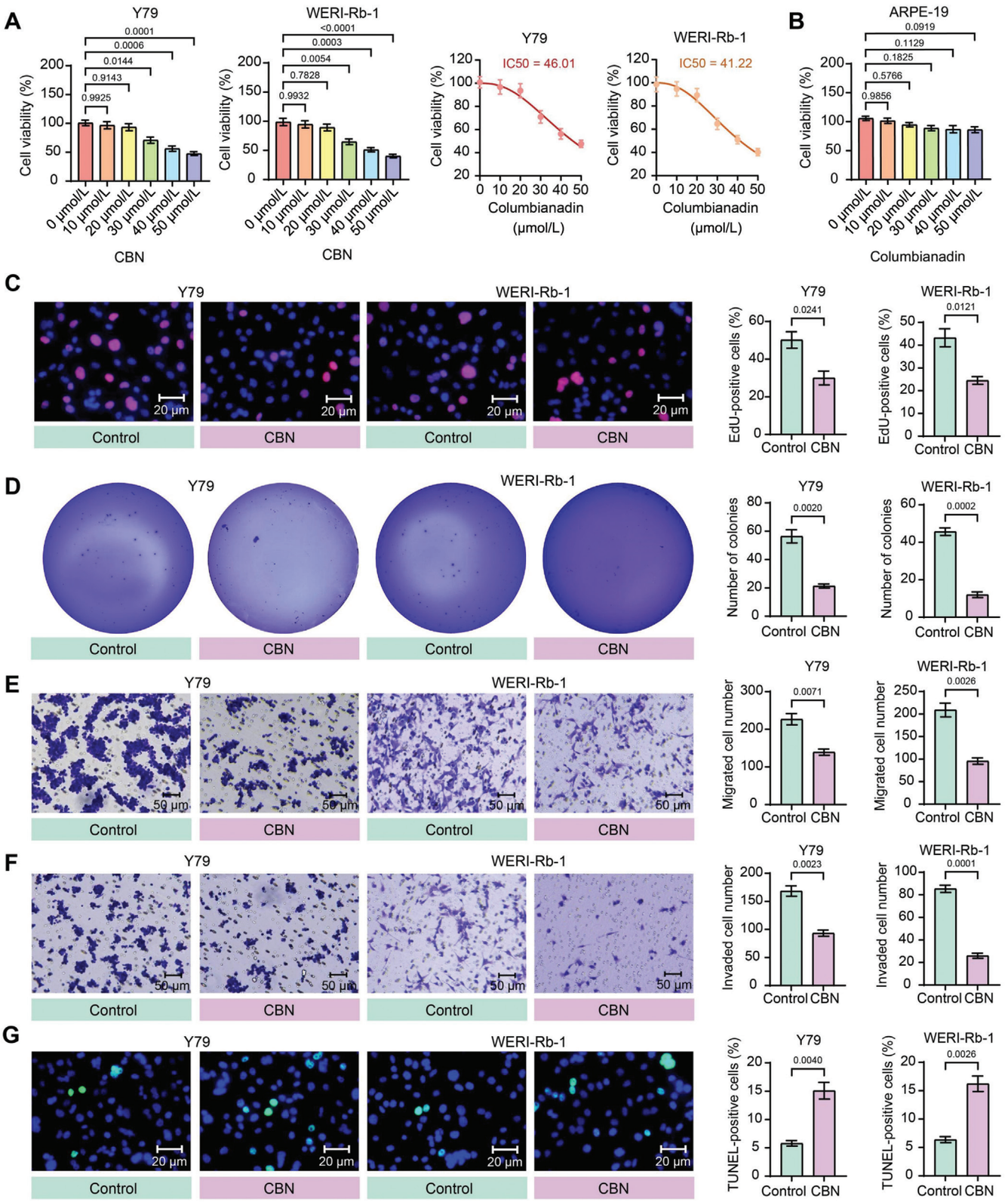


Figure 1 Inhibition of malignant phenotype and induction of apoptosis in RB cells by CBN A: Cell viability of RB cells treated with different concentrations of CBN was assessed by CCK-8 assay, and concentration-response curves were plotted for Y79 and WERI-Rb-1 cells to calculate IC_{50} values (*n*=3); B: ARPE-19 cell viability following treatment with different concentrations of CBN was examined by CCK-8 assay; C: Proliferation of RB cells following CBN treatment was evaluated by EdU assay (*n*=3); D: Colony-forming ability of RB cells after CBN treatment was assessed by soft agar assay (*n*=3); E–F: Migration and invasion abilities of RB cells after CBN treatment were detected by Transwell assay (*n*=3); G: The apoptosis rate of RB cells after CBN treatment was determined by TUNEL assay (*n*=3). Statistical analysis by one-way ANOVA (A–B), followed by Tukey's multiple comparisons test or unpaired *t*-test (C–G); *P*<0.05 was considered statistically significant. RB: Retinoblastoma; CBN: Columbianadin; CCK-8: Cell counting kit-8; EdU: 5-ethynyl-2′-deoxyuridine; TUNEL: Terminal deoxynucleotidyl transferase dUTP nick-end labeling; ANOVA: Analysis of variance.

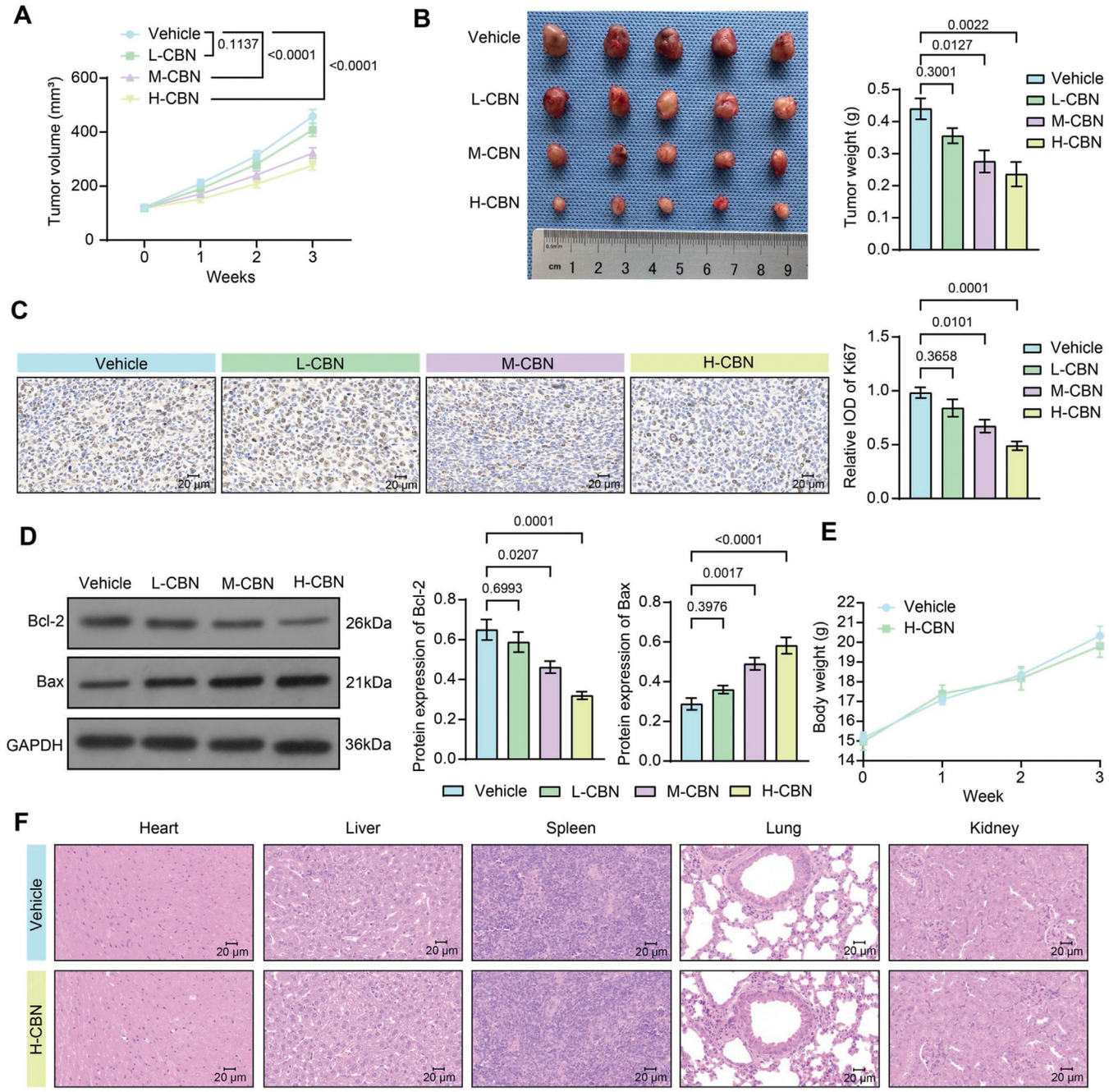


Figure 2 CBN exhibits antitumor activity *in vivo* and demonstrates preliminary systemic safety A: Tumor volume changes in mice administered with vehicle or low (L), moderate (M), and high (H) doses (n=5); B: Representative tumor images and tumor weight in each group (n=5); C: IHC analysis of Ki67 expression in tumor tissues (n=5); D: Protein expression of Bax and Bcl-2 in tumor tissues was detected by WB (n=5); E: Changes in body weight in normal nude mice during treatment with vehicle or H-CBN (n=5); F: The morphology of the heart, liver, spleen, lung, and kidney tissues in normal nude mice was observed using HE staining. Statistical analysis by one-way ANOVA (B–D) or two-way ANOVA (A, E), followed by Tukey's multiple comparisons test; P<0.05 was considered statistically significant. CBN: Columbianadin; IHC: Immunohistochemistry; IOD: Integrated optical density; WB: Western blotting; ANOVA: Analysis of variance; HE: Hematoxylin-eosin.

doses, high-dose CBN achieved the strongest antitumor effect *in vivo*; thus, this dose was used for subsequent studies.

Normal nude mice were treated with either vehicle or H-CBN (40 mg/kg) for a short-term safety assessment. Body weight data showed that no significant decrease in body weight was observed in nude mice during H-CBN treatment (Figure 2E). At the same time, HE staining results also indicated that H-CBN treatment did not cause significant pathological damage to the heart, liver, spleen, lung, or kidney tissues of nude mice (Figure 2F). This suggests that the maximum dose of CBN administered in this study did not result in any signs of organ toxicity.

CBN Suppresses TOP2A Protein Expression in RB Cells

To explore the underlying mechanism for the antitumor activity

of CBN in RB, the SMILES structure of CBN, C/C=C-(/C)\C(=O)OC(C)(C)[C@@H]1CC2=C(O1)–C=CC3=C2OC–(=O)C=C3 (PubChem CID: 6436246; Figure 3A) was obtained from PubChem using keyword "Columbianadin", and potential targets were predicted using Super-PRED (https://prediction.charite.de/index.php). Analysis of the GEO dataset GSE58780 identified differentially expressed genes between RB tumors (n=63) and fetal retina (n=3) using GEO2R with Benjamini–Hochberg correction ($adj.P$<0.01 and $|\log_2 FoldChange|$>1; Figure 3B). Intersecting the predicted CBN targets with these differentially expressed genes using Jvenn yielded 13 common genes (Figure 3C). STRING analysis (https://cn.string-db.org/) revealed that CDK1, CCNE1, TOP2A, and CDC25C had high protein-protein interaction (Figure 3D). Their expression in RB tissues in the GSE58780 dataset was as follows: TOP2A ($\log_2 FoldChange$=3.75759276), CDK1 ($\log_2 FoldChange$=3.61186087), CCNE1 ($\log_2 FoldChange$=2.40408356), and CDC25C ($\log_2 FoldChange$=1.71006358). TOP2A showed the most significantly aberrant expression, which was selected in our study. We hypothesized that CBN may inhibit RB progression by suppressing TOP2A.

WB confirmed that TOP2A was highly expressed in Y79 and WERI-Rb-1 cells compared with ARPE-19 cells (Figure 3E). CBN treatment markedly reduced TOP2A protein levels in RB cells (Figure 3F). Reverse transcription quantitative polymerase chain reaction (RT-qPCR) results showed that TOP2A mRNA expression in Y79 and WERI-Rb-1 cells did not change significantly following treatment with CBN (Figure 3G). Subsequently, to evaluate the potential binding affinity between CBN and TOP2A, we performed molecular docking analysis. CBN can stably interact with the TOP2A protein structure (PDB ID: 1ZXM), with an AutoDock Vina score of -9.814 kcal/mol for its optimal docking conformation. Further interaction analysis of the optimal binding conformation of CBN with TOP2A revealed that CBN is located within the predicted binding pocket of TOP2A, surrounded by key amino acid residues including Tyr34, Asn91, Ala92, Ile125, Ile141, Ser148, Ser149, and Asn150. Specifically, CBN forms hydrogen bonds with Ser148, Ser149, and Asn150; an amide–π-stacked interaction with the main-chain amide region of Asn91-Ala92; an alkyl interaction with Ile141; and π-alkyl hydrophobic interactions with Tyr34 and Ile125. In addition, van der Waals interactions may exist between CBN and the residues surrounding the binding pocket, which together contribute to the stability of the CBN-TOP2A complex (Figure 3H).

TOP2A Overexpression Reverses the Repressive Effects of CBN on the Malignant Behaviors of RB Cells To determine whether CBN suppresses RB cell proliferation, migration, invasion, and induces apoptosis *via* TOP2A inhibition, RB cell lines stably overexpressing TOP2A were generated *via* lentiviral infection and treated with CBN. WB confirmed successful overexpression of TOP2A (Figure 4A). Transwell assays revealed that TOP2A overexpression increased cell migration and invasion in the presence of CBN (Figure 4B, 4C). Soft agar assays showed that TOP2A overexpression enhanced RB cell colony formation (Figure 4D). EdU assays demonstrated accelerated proliferation with TOP2A overexpression (Figure 4E). TUNEL assays indicated that TOP2A overexpression suppressed CBN-induced apoptosis (Figure 4F).

CBN Suppresses the TOP2A Expression and PI3K/AKT Pathway in RB Cells We hypothesized that CBN may inhibit RB progression by suppressing TOP2A, thereby blocking the PI3K/AKT pathway. WB showed that CBN treatment decreased phosphorylation of PI3K and AKT in RB cells without affecting total PI3K and AKT levels; this effect was reversed by TOP2A overexpression (Figure 5A). Treatment with LY294002, the PI3K/AKT inhibitor, reduced p-PI3K and p-AKT levels without affecting total protein expression (Figure 5B). LY294002 treatment suppressed colony formation (Figure 5C), reduced proliferation (Figure 5D), impaired migration and invasion (Figure 5E, 5F), and promoted apoptosis (Figure 5G) in RB cells overexpressing TOP2A.

TOP2A Overexpression Attenuates the Antitumor Effects of CBN *in vivo* Y79 cells with lentiviral overexpression of TOP2A or a control vector were used to establish xenograft models in nude mice, followed by CBN treatment. TOP2A overexpression attenuated CBN-mediated tumor growth inhibition, as indicated by increased tumor volume and weight (Figure 6A, 6B). IHC showed that CBN reduced TOP2A expression in tumor tissues, whereas TOP2A overexpression restored its levels (Figure 6C). WB revealed that CBN inhibited p-PI3K and p-AKT levels in tumor tissues without affecting total protein levels, and these inhibitory effects were reversed by TOP2A overexpression (Figure 6D). IHC showed that TOP2A overexpression increased Ki67 expression in CBN-treated tumors (Figure 6E). Additionally, WB demonstrated that TOP2A overexpression increased Bcl-2 and decreased Bax expression in CBN-treated tumor tissues (Figure 6F).

DISCUSSION

RB is the most common malignant intraocular tumor in pediatric patients and poses a serious threat to survival if not promptly and effectively treated[15]. Plant-derived natural products have demonstrated notable therapeutic effects in the treatment of various tumors and have been widely investigated in RB research[16]. However, whether CBN exerts similar anticancer effects in RB remains to be elucidated.

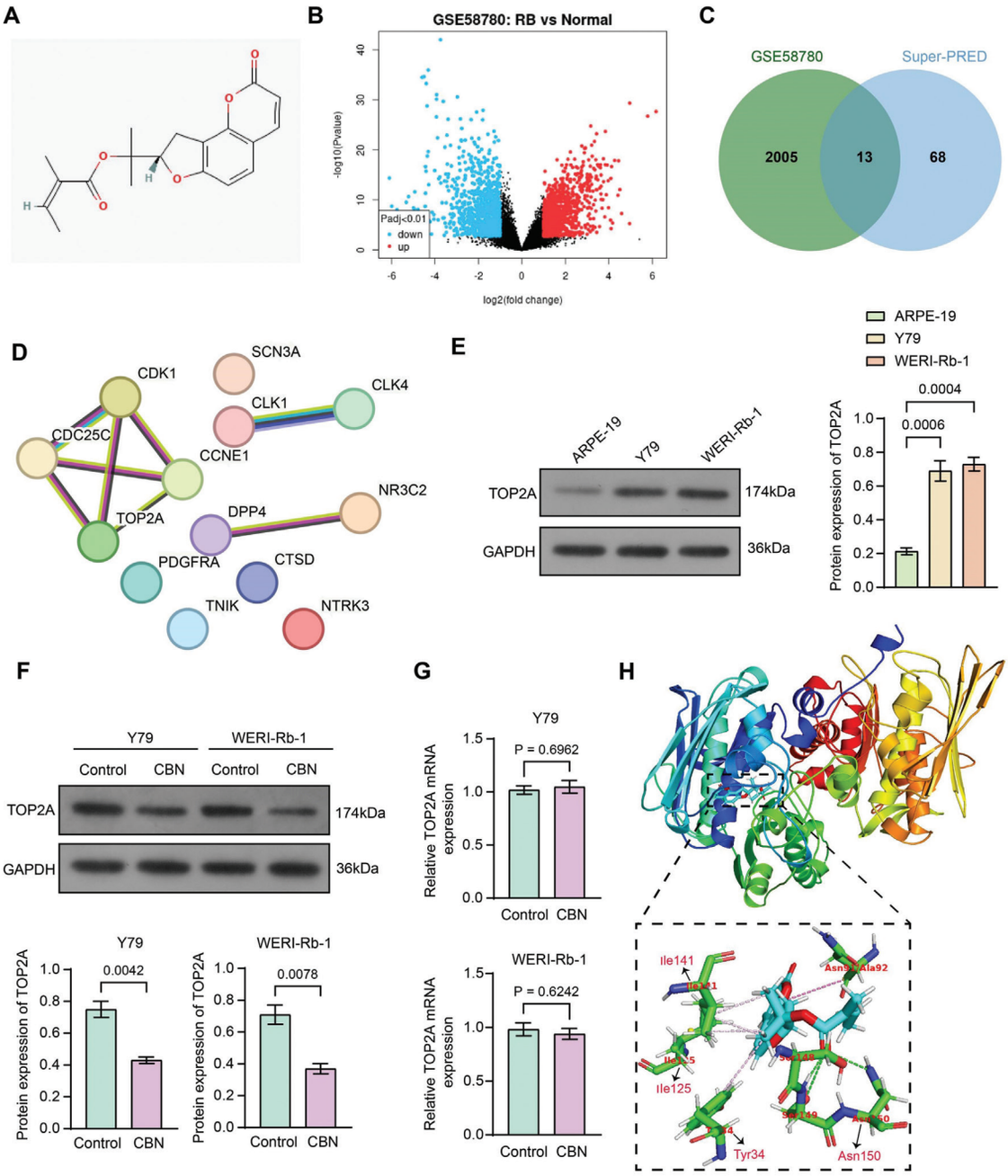


Figure 3 Suppression of TOP2A protein expression in RB cells by CBN A: SMILES structure of CBN obtained from PubChem (https://pubchem.ncbi.nlm.nih.gov/); B: Differentially expressed genes between RB tumors (*n*=63) and fetal retina (*n*=3) from the GSE58780 dataset, analyzed using GEO2R; C: Overlapping genes between predicted CBN target proteins and differentially expressed genes identified by Jvenn analysis; D: Protein-protein interaction network of overlapping genes analyzed by STRING; E: TOP2A expression in ARPE-19 cells and RB cells was detected by WB (*n*=3); F: TOP2A expression in RB cells after CBN treatment was detected by WB (*n*=3); G: RT-qPCR analysis of TOP2A mRNA expression in RB cells following treatment with CBN; H: Analysis of the optimal molecular docking conformation and local interactions between CBN and the TOP2A protein (PDB ID: 1ZXM). The dashed box indicates the predicted interaction zone for CBN. The enlarged image shows CBN fitting into the TOP2A binding pocket in a rod-like conformation; the surrounding key amino acid residues are labeled in the figure. Green dashed lines indicate hydrogen bonds, and purple dashed lines indicate hydrophobic interactions. Statistical analysis by one-way ANOVA (E), followed by Tukey's multiple comparisons test or an unpaired *t*-test (F–G); $P<0.05$ was considered statistically significant. TOP2A: DNA topoisomerase II alpha; RB: Retinoblastoma; CBN: Columbianadin; GEO: Gene Expression Omnibus; STRING: Search Tool for the Retrieval of Interacting Genes/Proteins; WB: Western blotting; ANOVA: Analysis of variance; RT-qPCR: Reverse transcription quantitative polymerase chain reaction.

Our results demonstrated that CBN markedly suppressed RB cell viability, proliferation, colony-forming ability, invasion, and migration, while promoting apoptosis. These findings are consistent with accumulating evidence that CBN exerts broad-spectrum anticancer activity by interfering with multiple malignant cell behaviors, such as in colon cancer cells[17]. The

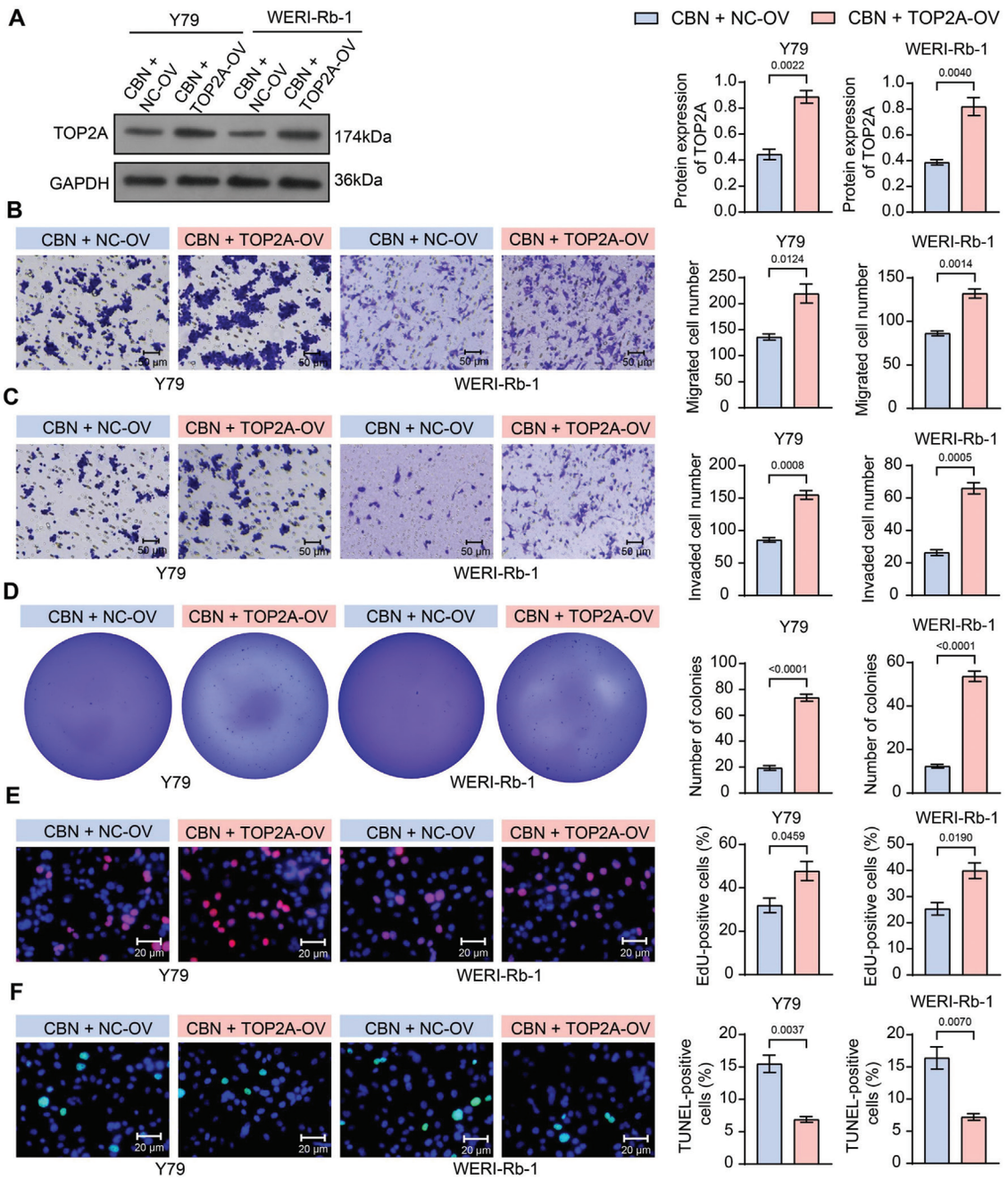


Figure 4 Reversal of CBN-mediated inhibition of malignant behaviors in RB cells by TOP2A overexpression A: Verification of TOP2A overexpression efficiency in RB cells by WB (*n*=3); B: Effect of TOP2A overexpression on RB cell migration by Transwell assay (*n*=3); C: Effect of TOP2A overexpression on RB cell invasion by Transwell assay (*n*=3); D: Effect of TOP2A overexpression on colony-forming ability of RB cells by soft agar assay (*n*=3); E: Effect of TOP2A overexpression on RB cell proliferation by EdU assay (*n*=3); F: Effect of TOP2A overexpression on RB cell apoptosis by TUNEL assay (*n*=3). Statistical analysis by unpaired *t*-test (A–F); $P<0.05$ was considered statistically significant. CBN: Columbianadin; RB: Retinoblastoma; TOP2A: DNA topoisomerase II alpha; WB: Western blotting; EdU: 5-ethynyl-2′-deoxyuridine; TUNEL: Terminal deoxynucleotidyl transferase dUTP nick-end labeling; ANOVA: Analysis of variance.

current study extended these observations to RB, indicating the inhibitory effects of CBN on tumor progression. In our study, CBN treatment reduced Ki67 expression in RB tumors. Our results align with prior findings showing that CBN, one of the compounds in periostracum cicadae, decreased Ki67 levels in gastric tissues[18]. Meanwhile, in our study, CBN increased Bax expression and decreased Bcl-2 levels, shifting the Bax/Bcl-2 ratio toward apoptosis. Additionally, the effective concentrations of CBN used in our experiments were within the range reported in previous cancer studies. For instance, CBN inhibited lung inflammation following oral administration at a dose of 20–60 mg/kg[19]. The acute toxicity assay indicated that the median lethal dose (LD_{50}) of CBN exceeded 2000 mg/kg[20]. *In vivo,* subcutaneous xenograft models of Y79 cells in nude mice treated with gradient doses of CBN (10, 20, and 40 mg/kg) also demonstrated inhibition of

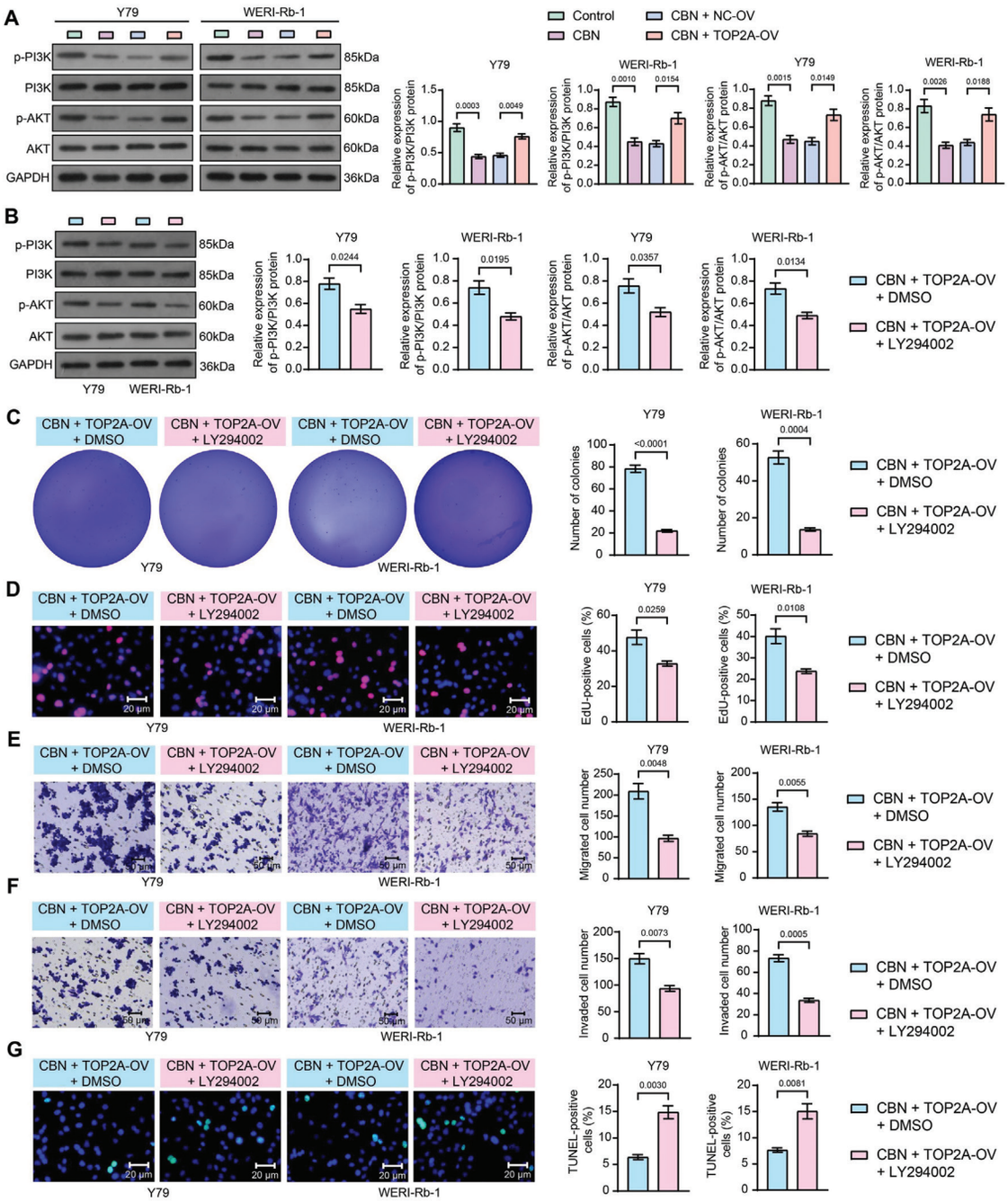


Figure 5 CBN inhibits the malignant behavior of RB cells by regulating TOP2A and the PI3K/AKT pathway A: The total protein and phosphorylation levels of PI3K and AKT in RB cells after CBN treatment and TOP2A overexpression were detected by WB (*n*=3); B: The total protein and phosphorylation levels of PI3K and AKT in RB cells after treatment with the PI3K/AKT inhibitor LY294002 were detected by WB (*n*=3); C: Colony formation of RB cells after LY294002 treatment was assessed by soft agar assay (*n*=3); D: Proliferation of RB cells after LY294002 treatment was evaluated by EdU assay (*n*=3); E: Migration of RB cells after LY294002 treatment was detected by a Transwell assay (*n*=3); F: Invasion of RB cells after LY294002 treatment was detected by a Transwell assay (*n*=3); G: Apoptosis of RB cells after LY294002 treatment was determined by TUNEL assay (*n*=3). Statistical analysis by one-way ANOVA (A), followed by Tukey's multiple comparisons test or unpaired *t*-test (B–G); $P<0.05$ was considered statistically significant. TOP2A: DNA topoisomerase II alpha; PI3K: Phosphoinositide 3-kinase; AKT: Protein kinase B; CBN: Columbianadin; RB: Retinoblastoma; WB: Western blotting; EdU: 5-ethynyl-2'-deoxyuridine; TUNEL: Terminal deoxynucleotidyl transferase dUTP nick-end labeling; ANOVA: Analysis of variance.

tumor growth, with notable reductions in both tumor volume and weight. High-dose CBN exhibited the strongest antitumor effect *in vivo* without significant organ toxicity.

Mechanistically, we identified TOP2A as a critical molecular target of CBN in RB. We detected elevated expression of TOP2A in RB, aligning with a previous study reporting that TOP2A is highly expressed in lung adenocarcinoma, breast cancer, and hepatocellular carcinoma[21]. Furthermore,

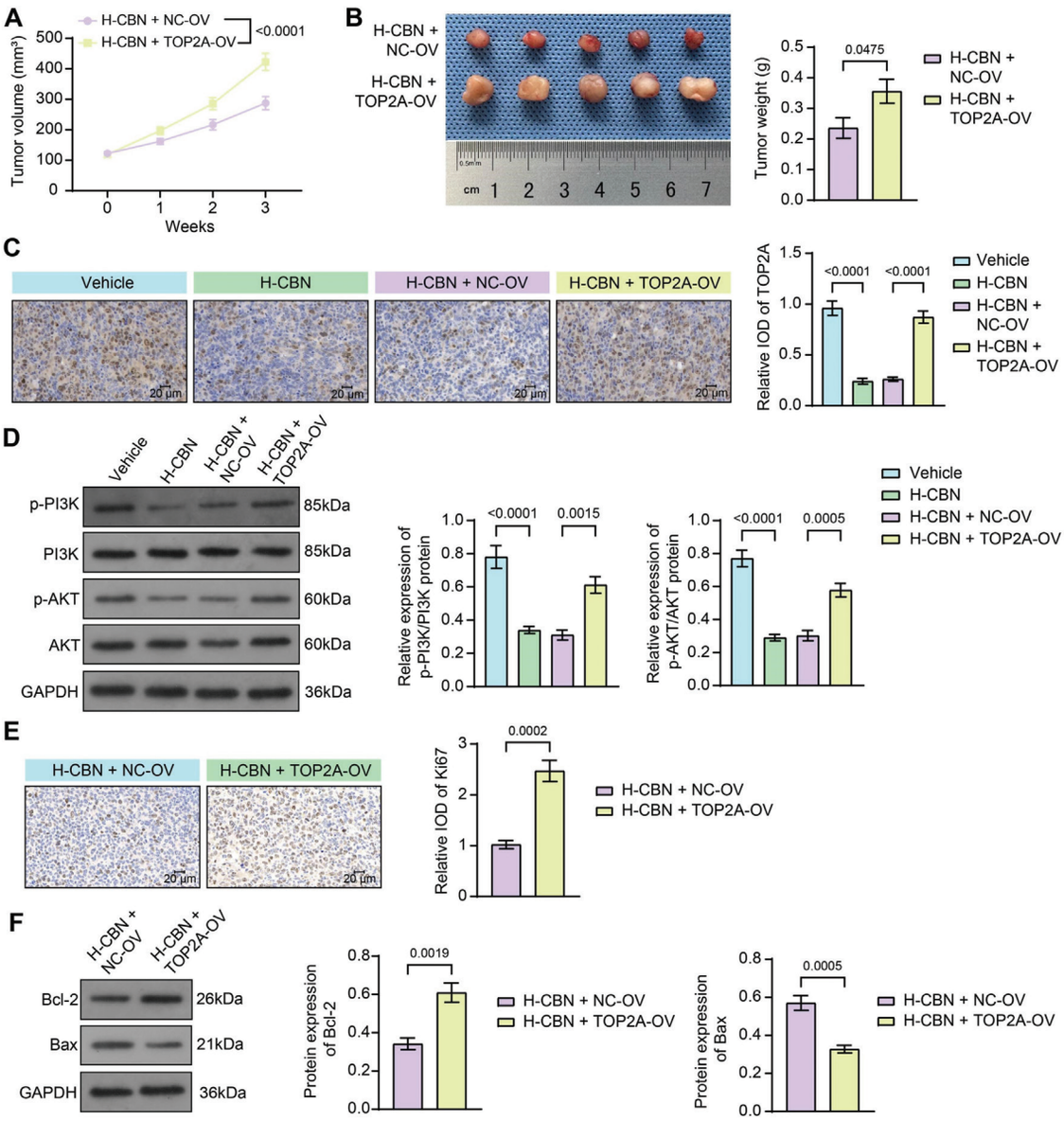


Figure 6 Attenuation of CBN-mediated tumor growth inhibition *in vivo* by TOP2A overexpression A: Tumor volume changes in xenograft models (*n*=5); B: Representative tumor images and tumor weight (*n*=5); C: TOP2A expression in tumor tissues (*n*=5) was detected by IHC; D: The total protein and phosphorylation levels of PI3K and AKT in tumor tissues (*n*=5) were detected by WB; E: Ki67 expression in tumor tissues (*n*=5) was detected by IHC; F: Protein expression of Bcl-2 and Bax in tumor tissues (*n*=5) was detected by WB. Statistical analysis by unpaired *t-tests* (B, E, F), one-way ANOVA (C–D), or two-way ANOVA (A), followed by Tukey's multiple comparisons test; *P*<0.05 was considered statistically significant. CBN: Columbianadin; TOP2A: DNA topoisomerase II alpha; IHC: Immunohistochemistry; IOD: Integrated optical density; PI3K: Phosphoinositide 3-kinase; AKT: Protein kinase B; WB: Western blotting; ANOVA: Analysis of variance.

TOP2A demonstrates elevated expression levels in high-grade serous ovarian cancer tissues and in cisplatin-resistant cells, which are strongly correlated with tumor progression, as indicated by advanced stage, high grade, and lymph node metastasis, and with a poor prognosis[22-23]. Knockdown of TOP2A induces apoptosis in non-small cell lung cancer cells[24]. Moreover, TOP2A may contribute to RB initiation, invasion, or recurrence[25]. It has been shown that natural compounds, including other plant-derived agents, can suppress TOP2A expression, thereby inhibiting tumor growth and enhancing apoptosis in breast cancer[26]. Abietic acid exhibited substantial antitumor effects in lung carcinoma by decreasing the expression of TOP2A[27]. Similarly, muscone suppresses TOP2A to promote mitochondrial-dependent apoptosis and restore chemosensitivity in temozolomide-resistant glioblastoma cells[28]. Our findings showed that CBN downregulated TOP2A protein levels in RB cell lines, suggesting that TOP2A may mediate the antitumor activity of CBN. Furthermore, TOP2A appeared to regulate the PI3K/AKT signaling pathway. In ovarian cancer, TOP2A knockdown suppresses proliferation, induces G1 arrest, and promotes apoptosis, accompanied by reduced p-AKT/AKT

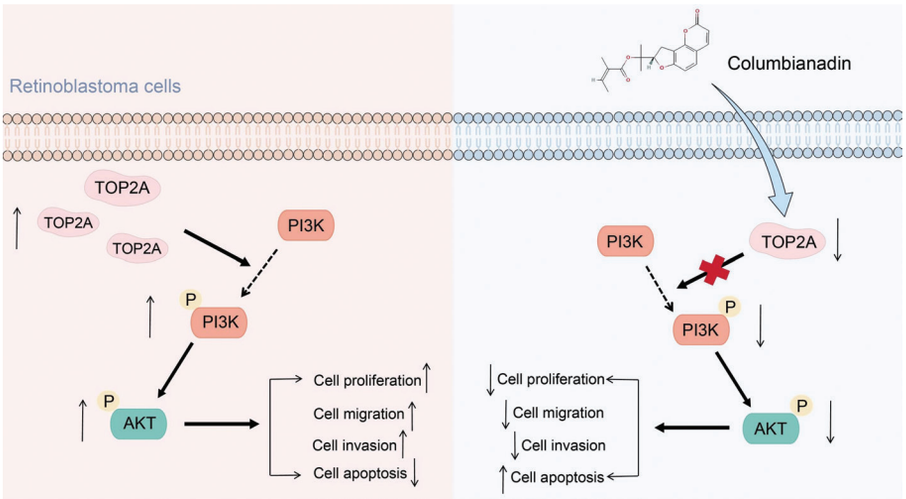


Figure 7 Schematic diagram CBN inhibits the malignant behaviors of RB cells by suppressing TOP2A protein expression and blocking activation of the PI3K/AKT signaling pathway. CBN: Columbianadin; RB: Retinoblastoma; TOP2A: DNA topoisomerase II alpha; PI3K: Phosphoinositide 3-kinase; AKT: Protein kinase B.

levels[29]. The PI3K/AKT signaling pathway is involved in the antitumor effects of Panax notoginseng saponins in RB cells[30]. Specifically, CBN has been shown to inhibit glioblastoma progression by suppressing PI3K/AKT signaling[8]. In our study, CBN treatment reduced phosphorylation of PI3K and AKT without affecting total protein levels, indicating suppression of pathway activity. Notably, overexpression of TOP2A partially reversed these inhibitory effects of CBN, restoring PI3K/AKT signaling and malignant phenotypes, both *in vitro* and in xenograft models.

This study still has three limitations that require further improvement. First, although the subcutaneous xenograft model is commonly used and acceptable for evaluating tumor growth, it does not fully recapitulate the intraocular microenvironment or metastatic behavior of human RB. Future studies employing orthotopic RB models or patient-derived xenografts may provide more physiologically relevant insights into the therapeutic potential of CBN. Second, the present findings indicate that TOP2A knockdown exerts a suppressive effect on PI3K/AKT signaling. However, the mechanistic link between a nuclear topoisomerase and a cytoplasmic signaling cascade remains incompletely understood. It is hypothesized that TOP2A may regulate the transcription of upstream activators of PI3K/AKT, including receptor tyrosine kinases, GPCRs, and integrins[9]. This indirect regulation of pathway activation is a potential mechanism through which TOP2A exerts its influence. Alternatively, stress-response pathways triggered by altered DNA replication/transcription may converge on PI3K/AKT. While the present data support a functional connection, further studies are required to identify the intermediate links and to rule out indirect effects. Finally, there are key translational issues to be resolved in addition to the demonstrated antitumor effects of CBN. It is imperative to consider systemic absorption and intraocular penetration as critical factors for ensuring sufficient concentrations of pharmaceutical agents within the ocular environment. Furthermore, the selection of the optimal delivery route, whether systemic administration, periocular injection, or direct intraocular delivery, will influence both efficacy and safety. Future studies should therefore investigate the pharmacokinetics and ocular bioavailability of CBN, as well as delivery strategies that maximize intraocular exposure while minimizing systemic toxicity.

Overall, our results establish TOP2A as a key mediator of RB malignancy and a target of CBN and highlight the PI3K/AKT pathway as a downstream effector of TOP2A in RB (Figure 7). These findings offer preliminary mechanistic insights into the antitumor activity of CBN and suggest that modulation of the TOP2A/PI3K/AKT axis may contribute to its therapeutic potential in RB.

ACKNOWLEDGEMENTS

Authors' Contributions: Li LJ: Conceptualization, methodology, investigation, formal analysis, writing–original draft. Sun H: Investigation, data curation, methodology. Tang ZH: Resources, software, validation. Xu MY: Conceptualization, supervision, project administration, writing –review & editing.

Data Availability Statement: The data used to support the findings of this study are available from the corresponding author upon request.

AI-Generated Content Disclosure: The authors declare that no artificial intelligence (AI) tools were used in the writing, analysis, or generation of any content in this manuscript.

Foundations: Supported by the National Science and Technology Basic Resources Survey Plan of the Ministry of Science and Technology (No.2019FY100502-4); the

General Program of Heilongjiang Postdoctoral Fund (No. LBH-Z20091); the Traditional Chinese Medicine Research Project of Heilongjiang Provincial Administration of Traditional Chinese Medicine (No.ZHY-20220138).

Conflicts of Interest: Li LJ, None; **Sun H,** None; **Tang ZH,** None; **Xu MY,** None.

REFERENCES

1 Byroju VV, Nadukkandy AS, Cordani M, *et al*. Retinoblastoma: present scenario and future challenges. *Cell Commun Signal* 2023;21(1):226.

2 Cruz-Gálvez CC, Ordaz-Favila JC, Villar-Calvo VM, *et al*. Retinoblastoma: review and new insights. *Front Oncol* 2022;12:963780.

3 Carnevale JA, Goldberg J, Kocharian G, *et al*. Intra-arterial chemotherapy for retinoblastoma. *J NeuroIntervent Surg* 2023;15(3):303-304.

4 Nag A, Khetan V. Retinoblastoma–a comprehensive review, update and recent advances. *Indian J Ophthalmol* 2024;72(6):778-788.

5 Raval V, Parulekar M, Singh AD. Emerging new therapeutics for retinoblastoma. *Ocul Oncol Pathol* 2022;8(3):149-155.

6 Wang N, Ke F, Li J, *et al*. Retinoblastoma management in China: clinical challenges. *Int J Ophthalmol* 2025;18(12):2380-2384.

7 Wang YS, Tang L, Miao J, *et al*. Pharmacological and pharmacokinetic insights into columbianadin: a promising natural anti-inflammatory compound. *Mediators Inflamm* 2025;2025:6284834.

8 Zhang W, Dong JH, Xu JY, *et al*. Columbianadin suppresses glioblastoma progression by inhibiting the PI3K-Akt signaling pathway. *Biochem Pharmacol* 2024;223:116112.

9 Uusküla-Reimand L, Wilson MD. Untangling the roles of TOP2A and TOP2B in transcription and cancer. *Sci Adv* 2022;8(44):eadd4920.

10 Zhu FJ, Wang PP, Zhang ZY, *et al*. Integrative genomic analysis reveals cancer-associated mutations in patients with ophthalmic tumors. *J Int Med Res* 2024;52(7):3000605241258171.

11 Xu XY, Lu XR, Liu X, *et al*. Novel β-carboline derivatives show promise as dual-target inhibitors of DNA and TOP2A for the treatment of triple negative breast cancer. *Eur J Med Chem* 2025;298:118041.

12 Wang ZP, Wang J, Chen S, *et al*. Chromatin regulators TOP2A and PPARGC1A stratify prostate cancer risk and reveal TOP2A-driven progression *via* PI3K/AKT pathway. *Chin J Cancer Res* 2026;38(1):83-99.

13 Li H, Jin CR. Retinoblastoma: unveiling molecular pathogenesis and pioneering organoid-driven therapeutic innovations. *Stem Cell Res Ther* 2026;17(1):96.

14 Niu ZC, An R, Shi HH, *et al*. Columbianadin ameliorates myocardial injury by inhibiting autophagy through the PI3K/Akt/mTOR signaling pathway in AMI mice and hypoxic H9c2 cells. *Phytother Res* 2025;39(1):521-535.

15 Zhou M, Tang JL, Fan JY, *et al*. Recent progress in retinoblastoma: pathogenesis, presentation, diagnosis and management. *Asia Pac J Ophthalmol (Phila)* 2024;13(2):100058.

16 Liu JC, Zhang CL, Dong KY, *et al*. Advances in the research of plant-derived natural products against retinoblastoma. *Int J Ophthalmol* 2022;15(8):1391-1400.

17 Kang JI, Hong JY, Choi JS, *et al*. Columbianadin inhibits cell proliferation by inducing apoptosis and necroptosis in HCT116 colon cancer cells. *Biomol Ther* 2016;24(3):320-327.

18 Liang H, Jin XF, He TT, *et al*. Investigation of c-fos/c-Jun signaling pathways in periostracum cicadae's inhibition of EMT in gastric tissue. *Pharmaceuticals* (*Basel*) 2025;18(4):537.

19 Lim HJ, Lee JH, Choi JS, *et al*. Inhibition of airway inflammation by the roots of Angelica decursiva and its constituent, columbianadin. *J Ethnopharmacol* 2014;155(2):1353-1361.

20 Chen SJ, Wang Y, Zhang L, *et al*. Therapeutic effects of columbianadin from Angelicae Pubescentis radix on the progression of collagen-induced rheumatoid arthritis by regulating inflammation and oxidative stress. *J Ethnopharmacol* 2023;316:116727.

21 Zhou T, Niu YT, Li YJ. Advances in research on malignant tumors and targeted agents for TOP2A (Review). *Mol Med Rep* 2025;31(2):50.

22 Liu XY, Wang JX, Liu YY, *et al*. Knockdown of TOP2A reverses cisplatin resistance in ovarian cancer by inhibiting EMT *via* ferroptosis mediated by the TP53/GPX4/SLC7A11 axis. *Front Immunol* 2025;16:1675373.

23 Mazzoleni V, Boichard A, Lamour V. DNA topoisomerase II mutations in cancer: structural impact and drug response in high-grade serous ovarian carcinoma. *J Mol Biol* 2026;438(5):169384.

24 Wu JT, Zhang L, Li WJ, *et al*. The role of TOP2A in immunotherapy and vasculogenic mimicry in non-small cell lung cancer and its potential mechanism. *Sci Rep* 2023;13(1):10906.

25 Huang J, Zhang LR, Li ZM, *et al*. Screening and identification of key biomarkers for retinoblastoma: evidence from bioinformatics analysis. *Medicine* 2020;99(20):e19952.

26 Mehraj U, Qayoom H, Shafi S, *et al*. Cryptolepine targets TOP2A and inhibits tumor cell proliferation in breast cancer cells-*an in vitro* and *in silico* study. *Anticaucer Agents Med Chem* 2022;22(17):3025-3037.

27 Zhu ZY, Gu J, Liao ZH, *et al*. Abietic acid induces DNA damage and cell apoptosis in lung cancer cells through targeting TOP2A. *Biomolecules* 2025;15(11):1498.

28 Zou YH, Xu LY, Wang WY, *et al*. Muscone restores anoikis sensitivity in TMZ-resistant glioblastoma cells by suppressing TOP2A *via* the EGFR/Integrin β1/FAK signaling pathway. *Phytomedicine* 2024;129:155714.

29 Zhang KW, Zheng XY, Sun YQ, *et al*. TOP2A modulates signaling *via* the AKT/mTOR pathway to promote ovarian cancer cell proliferation. *Cancer Biol Ther* 2024;25(1):2325126.

30 Liu JC, Zhang CL, Jia BY, *et al*. Panax notoginseng saponins induce apoptosis in retinoblastoma Y79 cells *via* the PI3K/AKT signalling pathway. *Exp Eye Res* 2022;216:108954.